AGU100 ADVANCING EARTH AND SPACE SCIENCE

Geophysical Research Letters

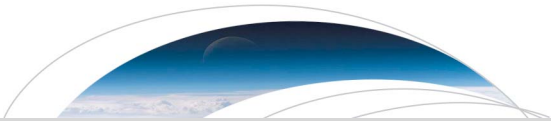

RESEARCH LETTER
10.1029/2018GL079956

Key Points:
- Formulation of autoconversion was found to determine the manner of warm-rain formation and the occurrence of nonprecipitating clouds
- Process-based constraint on warm rain was found to cause overly negative aerosol indirect effect in a GCM
- The overestimation of the AIE stems from a pronounced cloud-water response to aerosol that is amplified via the rain-scavenging interplay

Supporting Information:
- Supporting Information S1

Correspondence to:
X. Jing,
jing_xw@aori.u-tokyo.ac.jp

Citation:
Jing, X., & Suzuki, K. (2018). The impact of process-based warm rain constraints on the aerosol indirect effect. *Geophysical Research Letters*, *45*, 10,729–10,737. https://doi.org/10.1029/2018GL079956

Received 27 FEB 2018
Accepted 23 SEP 2018
Accepted article online 27 SEP 2018
Published online 10 OCT 2018

The Impact of Process-Based Warm Rain Constraints on the Aerosol Indirect Effect

Xianwen Jing[1] and **Kentaroh Suzuki**[1]

[1]Atmosphere and Ocean Research Institute, University of Tokyo, Kashiwa, Japan

Abstract Many global climate models have been found to generate warm rain too frequently. This study, with a particular global climate model, found that the problem can be mitigated via altering the autoconversion process so as to inhibit rain formation under conditions of a large cloud number concentration and small droplet sizes. However, this improvement was found to cause an overly large aerosol indirect effect. This *dichotomy* between the constraint on warm-rain formation process and the energy-budget requirement on aerosol indirect effect was found to result from a pronounced cloud-water response to aerosol perturbations, which is amplified through the wet scavenging feedback to an extent depending on precipitation-formation parameterization. Thus, critical compensating errors exist between warm-rain formation and other key processes, and better constraint on these processes, particularly wet scavenging, is required to mitigate the dichotomy. The results have broad implication for models that suffer from the aforementioned too-frequent warm-rain formation bias.

Plain Language Summary Climate scientists rely on numerical climate models to project temperature changes in the coming decades. The credibility of the projections is argued to arise from the fact that models are able to reproduce well the temperature trend in the past century. However, success in reproducing the past does not necessarily mean credible projection for the future, because the former may be a result of compensating biases in the models, which potentially misrepresent the relationship between changes to the energy balance and aerosols/clouds. In this study, compensating biases were found to exist between rain formation and other processes in a model capable of simulating aerosol effects. Specifically, this model tends to generate rain too frequently against satellite observations, whereas satellite-based improvements with respect to the rain process yield an unrealistically strong aerosol indirect effect that can substantially cool the surface. This means that dual efforts are required to derive trustworthy projections of future climate changes: on the one hand, the rain-formation process should be represented realistically in accordance with observations, while on the other hand, errors in the interaction between rain and aerosol/cloud should be mitigated.

1. Introduction

Global climate models (GCMs) are commonly constrained according to historical-period energy budgets at the top of the atmosphere (TOA) before they are used to predict future climate changes induced by anthropogenic forcing agents (e.g., aerosols and greenhouse gases; Eyring et al., 2016). However, even though they represent the historical temperature record well, a growing body of evidence shows that models suffer from substantial biases in their process representations, such as those relevant to the interaction among aerosol, cloud, and precipitation (Stephens et al., 2010; Suzuki et al., 2015; Takahashi et al., 2017). These process-level biases may cause erroneous prediction of the climate response to anthropogenic forcings, and this could be a major reason for the vast diversity in the future temperature trend projected by multiple GCMs (Collins et al., 2013).

One particular process that is poorly represented in GCMs is the warm (i.e., liquid) precipitation formation, which has been found in state-of-the-art GCMs to commonly occur too readily and too frequently (Jing et al., 2017; Stephens et al., 2010) compared with satellite observations, despite the accumulated surface precipitation amount being comparable to observations. The representation of the warm-rain formation process exerts considerable influence on aerosol indirect effect (AIE; Golaz et al., 2011), which is a substantial controlling agent for global mean surface temperature (Rotstayn et al., 2015).

The bias of precipitation occurrence in some models has been shown to be partly due to the unrealistically small threshold of cloud droplet effective radius (R_e) for the onset of warm precipitation (Golaz et al.,

2011). Correcting this bias in some GCMs by applying an observation-based threshold of R_e and simultaneously retuning the model to achieve the required energy budget, however, has been demonstrated to significantly enhance the energy sensitivity to aerosol perturbations, mainly through the AIE (Menon et al., 2002; Rotstayn, 2000), even to the extent that it could cancel much of the 20th century warming (Golaz et al., 2013; Suzuki et al., 2013).

The enhancement in the AIE caused by inhibited warm-rain formation at a smaller R_e implies a dichotomy between improving the warm-precipitation formation process and the energy budget requirement on the AIE due to aerosol perturbations (hereafter referred to as P&E dichotomy): restricting the onset of warm rain is likely to result in a larger AIE. Given the common bias of too-frequent warm-rain formation among many GCMs, this P&E dichotomy revealed from a few models is worth exploring in more models.

This study explores the relationship between the precipitation-formation process and AIE by applying two distinctive warm-rain formation formulations, unlike altering the threshold of R_e in the above studies, in the Model for Interdisciplinary Research on Climate version 5.2 (MIROC5.2; Watanabe et al., 2010), coupled with the Spectral Radiation-Transport Model for Aerosol Species (SPRINTARS; e.g., Takemura et al., 2009). SPRINTARS has been shown to yield a smaller dependency of cloud water on aerosol perturbations than other models, to an extent that is dependent on autoconversion formulations (Ghan et al., 2016). We examine the process-level behavior of warm rain against a satellite-based metric and explore its effect on the anthropogenic AIE from the preindustrial (PI) to present-day (PD) period. Particular emphasis is placed on the role of aerosol-cloud coupling through wet scavenging in determining the AIE. This study provides insights into how the warm-rain formation process manipulates the AIE and what the P&E dichotomy found in some models implies for others.

2. Data, Model, and Methods

2.1. Satellite Data

For evaluation of the simulated precipitation process, satellite data from CloudSat (Marchand et al., 2008) and the Moderate Resolution Imaging Spectroradiometer (MODIS; Platnick et al., 2015) onboard the A-Train constellation from 2007 to 2010 are used. Radar reflectivity from the CloudSat 2B-GEOPROF product is employed to obtain the vertical profiles within clouds. Cloud top R_e, cloud top temperature (T_{ctop}), and cloud optical depth (τ_c) from the Aqua MODIS products (MYD06_L2) are also employed and collocated to the CloudSat footprint. The cloud properties from MODIS are used to separate warm (i.e., liquid) and cold (i.e., ice) clouds and to track the evolution of precipitation.

2.2. Model Description

MIROC5.2 coupled with the SPRINTARS aerosol module is used in this study. MIROC5.2 has a standard horizontal resolution of T85 (about 1.4°) and a vertical resolution of 40 layers up to about 3 hPa and can be run with a coupled ocean model or with prescribed sea surface temperature (SST). Full aerosol-cloud interactions are considered in SPRINTARS, including all the main tropospheric aerosol types and two-moment bulk microphysics for cloud droplets and ice crystals (Takemura et al., 2009).

The default warm-rain formation scheme of MIROC5.2 is from Berry (1968; hereinafter BR68). An alternative scheme, from Khairoutdinov and Kogan (2000; hereinafter KK00), is implemented here. The two schemes are characterized by significantly different precipitation time scales (Michibata & Takemura, 2015; Suzuki et al., 2015). The autoconversion rates (R_{aut}, $\mathrm{kg \cdot m^{-3} \cdot s^{-1}}$) are given as follows:

$$\mathrm{BR68}: \quad R_{\mathrm{aut}} = \frac{3.5\times10^{-2}L_c^2}{0.12 + 1.0\times10^{-12}\frac{N_c}{L_c}}; \tag{1}$$

$$\mathrm{KK00}: \quad R_{\mathrm{aut}} = f_{\mathrm{tune}}\times1,350L_c^{2.47}\left(N_c\times10^{-6}\right)^{-1.79}\rho_a^{-1.47}. \tag{2}$$

Here L_c is the liquid water content ($\mathrm{kg/m^3}$), N_c is the cloud droplet number concentration ($\mathrm{m^{-3}}$), and ρ_a is the air density ($\mathrm{kg/m^3}$). Both L_c and N_c are prognostic variables within the two-moment scheme. f_{tune}, equaling 5.0 here, is an additional tuning factor to the original KK00 equation, aimed at achieving a TOA energy budget comparable to the default BR68 simulation (targeting ±1.0 $\mathrm{W/m^2}$ for the PI simulation). This tuning of KK00

affects only the overall magnitude of R_{aut} and retains the functional dependency of R_{aut} on L_c and N_c. No other tuning is made to exclude inconsistency in other parts of the model.

2.3. Methods

2.3.1. Warm-Rain Formation Process Assessment

For comparisons with satellite observations in the context of the warm-rain process, the Cloud Feedback Model Intercomparison Project Observation Simulation Package (COSP) version 2.0 (Swales et al., 2018) is applied to translate model cloud fields into observation-like radar reflectivity computed at subcolumns defined within model grids.

A 1-year simulation with COSP under PD aerosol emissions is conducted for each autoconversion scheme and analyzed in comparison to A-Train observations. Model results are output as six-hourly snapshots and then sampled according to local time (01:00–02:00 and 13:00–14:00) at each grid point to approximately match A-Train's equator crossing time (~01:30 and ~13:30).

The precipitation process is assessed with the Contoured Frequency by Optical Depth Diagram (CFODD) method (Nakajima et al., 2010; Suzuki et al., 2010), which *fingerprints* the transition of the vertical microphysical structure from a nonprecipitating to precipitating cloud regime as a fairly monotonic function of R_e. A brief description of how a CFODD is constructed is provided in section 3.1.

2.3.2. AIE Analysis

To investigate the effect of warm-rain formulations on the anthropogenic AIE, a pair of 15-year simulations with PI and PD aerosol emissions is conducted for each autoconversion scheme. Since our focus is on the AIE, which happens on a rapid time scale without interaction with SST, prescribed SST is used. Greenhouse gases are held at their PI magnitudes in both the PD and PI experiments. The first and second AIEs (Albrecht, 1989) are not separated because we are concerned with the overall energy budget changes due to aerosol-cloud interaction.

The anthropogenic AIE is diagnosed, following Ghan (2013), as AIE = $\Delta(F_{clean} - F_{clear,\ clean})$, in which F_{clean} and $F_{clear,\ clean}$ are the all-sky and clear-sky radiative fluxes at the TOA, respectively, calculated by neglecting the aerosol optical depth (AOD), and Δ means the difference between the PD and PI simulations (PD − PI).

The PI simulations under the BR68 and KK00 schemes feature analogous 15-year mean states of clouds, precipitation, and energy budgets (see Table S1 and Figure S1). Thus, the differences in the anthropogenic AIE between the two schemes illustrate the warm rain-induced variations in energy sensitivity to aerosol perturbations, which is crucial for future climate projections.

2.3.3. Effect of Wet Scavenging on the AIE

Additional simulations are conducted to isolate the role of aerosol wet-scavenging in influencing the AIE (section 3.3). In these simulations, a fixed N_c is used for the calculation of the precipitation flux used in the wet-scavenging process; meanwhile, the aerosol-mediated N_c is used in the cloud microphysics to derive the precipitation flux transmitted to other parts of the model. Since the N_c is the pathway by which aerosols influence precipitation (equations (1) and (2)), a fixed N_c for the precipitation in wet scavenging makes the wet removal of aerosols insensitive to aerosol-induced variations in cloud properties, and thus turns off the feedback to the AIE from the changes in wet scavenging. Nevertheless, the use of the aerosol-mediated N_c in cloud microphysics maintains the connection between precipitation's depletion of cloud water and aerosol concentrations.

These additional simulations are integrated for 15 model years and denoted as BR68_FN and KK00_FN, respectively. Different fixed N_c values, ranging from 1.0×10^7 to $1.2 \times 10^8/m^3$, are tested (the N_c distribution of the droplet population and the location of the fixed N_c values are shown in Figure S4); the results using an intermediate value ($N_c = 3.0 \times 10^7/m^3$) are mainly reported here.

3. Results and Discussion

3.1. Warm-Rain Formation Process

We begin by investigating the precipitation-formation process of the PD simulations. We employ CFODD to fingerprint the precipitation process in clouds. CFODD computes the probability distribution function of radar reflectivity in each bin of in-cloud optical depth (ICOD) and displays the statistics for all ICOD bins in

the form of a contoured frequency diagram. For observations, the MODIS τ_c with an adiabatic growth assumption algorithm (Suzuki et al., 2010) is used to determine the vertical profile of ICOD. For the model results, the radar reflectivity and τ_c are derived from COSP, and the ICOD is obtained with the adiabatic growth algorithm. Only warm clouds (defined by $T_{ctop} > 0\ ^{\circ}C$) are considered in the analysis.

Figures 1a–1i show the CFODD statistics over the global ocean, classified according to cloud top R_e ranges (5–10, 10–15, and 15–20 μm). The statistics of the A-Train (Figures 1a–1c) shift monotonically from nonprecipitating profiles (radar reflectivity < -15 dBZ) to raining profiles (radar reflectivity >0 dBZ) with increasing R_e, as previously found by Suzuki et al. (2010). The intermediate range of reflectivity (−15–0 dBZ), prevailing in Figure 1b in the lower part of clouds, is usually regarded as indicating the occurrence of light rain (i.e., drizzle; e.g., Haynes et al., 2009). This suggests that the onset of drizzle probably occurs in the R_e range of 10–15 μm, consistent with findings from in situ observations (Boers et al., 1998; Pawlowska & Brenguier, 2003). For clouds with sufficiently small particle sizes ($R_e < 10$ μm; Figure 1a), precipitation is very unlikely to happen even if the cloud optical depth develops to a considerable magnitude.

However, the simulation with BR68 (Figures 1d–1f) shows precipitating profiles even in the smallest R_e range (with radar reflectivity as large as ~0 dBZ). This demonstrates that BR68 generally lacks nonprecipitating clouds and even the drizzle mode of precipitation. Precipitation readily occurs and reaches considerable efficiency, regardless of cloud droplet size.

KK00, on the other hand, is significantly closer to the observations than BR68 in the smallest R_e range (Figure 1g). Considerably more nonprecipitating clouds and virtually no raining clouds are seen in this range, which is also analogous to the results of applying KK00 in other GCMs (Suzuki et al., 2015). This suggests that the implementation of KK00 in MIROC5.2 actually inhibits the formation of precipitation when the R_e is small, especially in the polluted clouds, taking on the process-level behavior of precipitation closer to satellite observations.

The inhibition of precipitation by KK00 in polluted regions, bringing the behavior of precipitation closer to the satellite observations, stems not from using a proper threshold of R_e (no threshold of R_e is used in this study), but from its proportional dependence of the autoconversion rate on the L_c and N_c (Figures 1j–1k), especially the larger negative dependence on the N_c ($R_{aut} \propto N_c^{-1.79}$ for KK00 and $R_{aut} \propto N_c^{-1.0}$ for BR68) that substantially decelerates the cloud-to-precipitation transition when the N_c is large (as indicated by the negative R_{aut} differences in Figure 1l, and also the smaller R_{aut} for KK00 than for BR68 at large N_c values for a given L_c in Figure S2). This is corroborated by the fact that the increase in nonprecipitating clouds of KK00 occurs mostly in regions with high aerosol loadings and thus a high N_c (Figure S3).

3.2. AIE

Next, we investigate the impacts of the above changes on the anthropogenic AIE. Figure 2a shows the simulated AIEs with the BR68 and KK00 autoconversion schemes (red and blue solid fill, respectively), as well as the expert judgment in Intergovernmental Panel on Climate Change Fifth Assessment Report (IPCC AR5; Myhre et al., 2013; gray solid fill). MIROC5.2 with BR68 gives an AIE of -1.06 W/m^2, which is slightly larger than the IPCC AR5 estimate (-0.45 W/m^2, with a 90% uncertainty range from 0 to -1.2 W/m) but still within its uncertainty range. This is not unexpected, since MIROC5.2 with BR68 (the default model configuration) has been well *tuned* for historical simulation. In contrast, the AIE obtained with KK00 is as large as -3.05 W/m^2; such a large negative forcing could offset much of the greenhouse-effect warming (equivalent to a forcing of +3.00 [2.22 to 3.78] W/m^2; Myhre et al., 2013) in the last century.

The *overestimate* of the AIE with a better representation of the warm-rain formation process indicates that the P&E dichotomy already apparent in other models, such as the Commonwealth Scientific and Industrial Research Organisation (CSIRO)'s GCM (Rotstayn, 2000) and Geophysical Fluid Dynamics Laboratory Coupled Model 3 (GFDL CM3; Golaz et al., 2013), also occurs in MIROC5.2. There are some common points between this study and those previous ones in that they all postponed the onset of warm rain and thus mediated the too-frequent warm-rain bias (whether by altering the threshold of R_e or by modifying the autoconversion function), and retuned the model to the required energy budget but ultimately saw substantial increases in the AIE for PD–PI aerosol perturbations. These common points are unlikely to be a mere coincidence. They imply compensating biases between warm-rain formation and other processes.

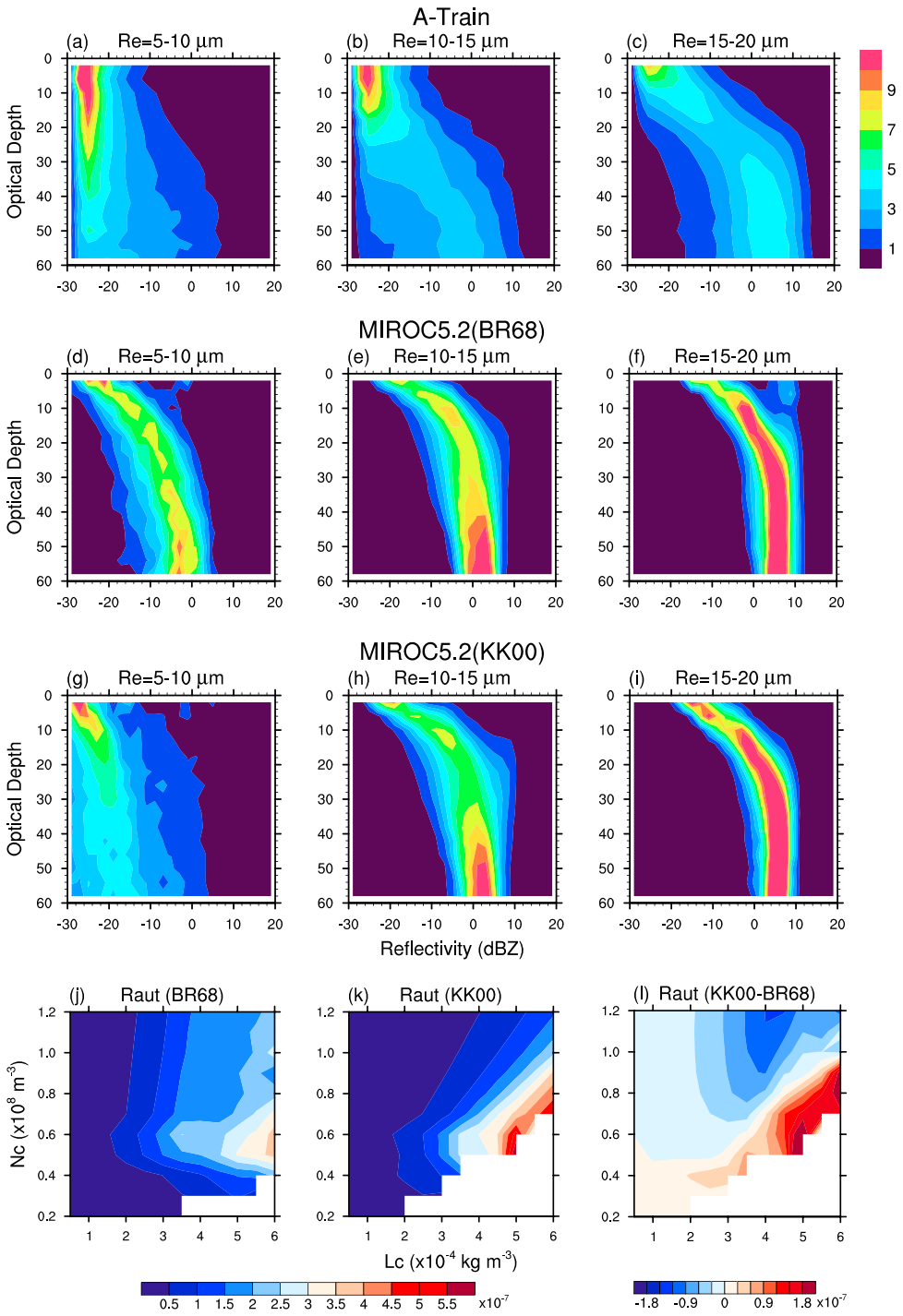

Figure 1. Probability distribution function of radar reflectivity as a function of in-cloud optical depth (i.e., Contoured Frequency by Optical Depth Diagrams [CFODDs]) for (a–c) the A-Train, (d–f) Model for Interdisciplinary Research on Climate version 5.2 (MIROC5.2) with BR68 autoconversion, and (g–i) MIROC5.2 with KK00 autoconversion, as well as the autoconversion rate ($kg \cdot m^{-3} \cdot s^{-1}$) as a function of the liquid water content and cloud droplet number concentration from the (j and k) two MIROC5.2 simulations and (l) their differences. For the CFODDs, the numbers of bins for optical depth and reflectivity are 15 and 25, respectively, and the radar reflectivity is normalized in each bin of in-cloud optical depth.

It could be argued that the large AIE just means that other *tunable parameters* should be further retuned to reduce the model sensitivity to aerosol perturbations; however, we regard the P&E dichotomy as being related to more fundamental issues, such as the absence of mechanisms involved in aerosol-cloud-

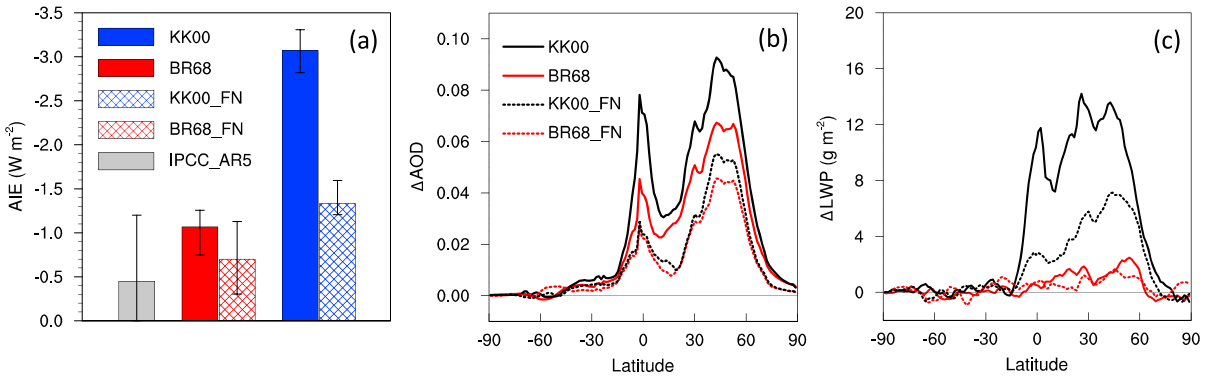

Figure 2. (a) The anthropogenic aerosol indirect effect from estimates of Intergovernmental Panel on Climate Change Fifth Assessment Report (IPCC AR5; gray) and those from the default simulations of Model for Interdisciplinary Research on Climate version 5.2 (MIROC5.2) with the BR68 (red, solid fill) and KK00 (blue, solid fill) autoconversion schemes, as well as those from the fixed-N_c wet-scavenging experiments BR68_FN (red, grid fill) and KK00_FN (blue, grid fill). The error bar for IPCC AR5 indicates the uncertainty range, while those for the model results indicate the maximum and minimum annual mean values in the 15-year simulations. (b and c) The differences in the zonal annual mean AOD and LWP, respectively, between the preindustrial (PI) and present-day (PD) simulations for each of the above model configurations.

precipitation interactions. Specifically, attention should be paid to those mechanisms affecting the susceptibility of cloud water to aerosols. Large-scale GCMs, including MIROC5.2 and GFDL CM3, generally show monotonic increases in cloud water with increasing aerosol loadings (Michibata et al., 2016; Zhao et al., 2018), but observations have also shown a negative relationship between them for some cloud regimes or regions (Malavelle et al., 2017; Matsui et al., 2006; Sato et al., 2018; Small et al., 2009), which buffers the cloud response to aerosol perturbations and results in a smaller AIE than estimated by GCMs (Stevens & Feingold, 2009). Such mechanisms that could lead to reduced cloud-water susceptibility to aerosols—for example, the evaporation and condensation processes of cloud particles, as suggested by a global cloud resolving model (Sato et al., 2018), mixed-phase and ice-cloud microphysics that could lead to a positive lifetime effect (Storelvmo et al., 2008), and updraft within clouds (Donner et al., 2016)—operate mostly at subgrid scales. Although fine-resolution models (e.g., Jiang et al., 2006; Sato et al., 2018) or multiscale modeling framework models (Wang et al., 2011) have captured some features of these processes, it remains a challenge to represent them in conventional GCMs due to scale disparity.

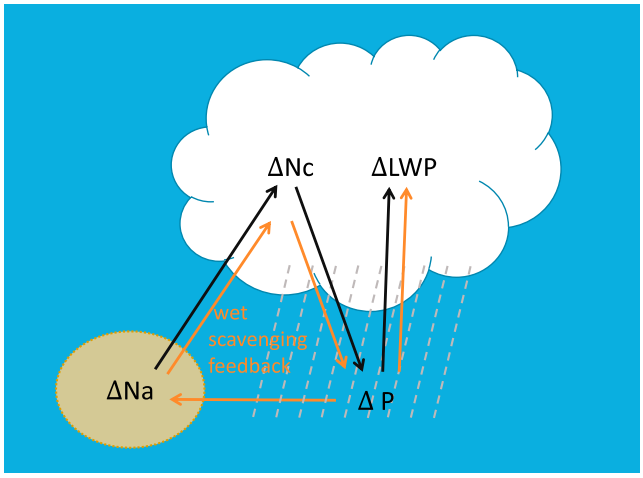

Figure 3. Schematic representation of the effects of aerosol-induced changes in precipitation on cloud properties, wherein Δ denotes the changes from the base state. The black arrows indicate the initial effects of aerosol variations (ΔN_a) on the LWP through changes in the N_c, and thus the depletion efficiency of precipitation (P). The orange arrows indicate the aerosol wet-scavenging feedback.

3.3. Feedback of Wet Scavenging to the AIE

By increasing aerosols in the atmosphere, the parameterizations in GCMs generally inhibit precipitation formation due to the larger N_c and smaller R_e and, hence, less efficient coalescence of cloud particles. This lifetime effect contributes most of the difference in the AIE between KK00 and BR68, as implied by their large difference in the ΔLWP (i.e., the PD-PI difference in liquid water path; Table S1). The inhibited precipitation in regions with increased aerosols induces changes in two aspects: (1) cloud water—the inhibition of precipitation initially decreases the depletion of cloud water, resulting in a larger LWP, and (2) aerosol—the inhibition of precipitation also decreases the wet scavenging of aerosols, causing a larger aerosol loading in the atmosphere, which further feeds back to cloud/precipitation properties through their mutual interaction. The processes of these two aspects of change are illustrated in Figure 3 by the black and orange arrows, respectively.

The additional simulations with a fixed N_c (see section 2.3.3) are conducted in order to isolate the role of wet-scavenging feedback in influencing the AIE. The grid bars in Figure 2a show the simulated anthropogenic AIEs from the $N_c = 3 \times 10^7/m^3$ experiments. It is shown that the global mean AIE of KK00_FN (−1.00 W/m^2), which does not include the wet-scavenging feedback, is considerably smaller than the default KK00

experiment. If the fixed N_c value is set as smaller but more representative values, the AIE of KK00_FN becomes even smaller (Figures S4 and S5). The smaller AIE is associated with much smaller ΔAOD and ΔLWP due to anthropogenic aerosol perturbations (Figures 2b and 2c, blue lines). These imply that under the KK00 autoconversion scheme, the interplay between aerosol-induced changes in precipitation and the wet scavenging of aerosols plays a crucial role in determining the cloud-water response and AIE. Specifically, their interplay amplifies the LWP response to, and the AIE of, aerosol perturbations. The amplification effect on the AIE is also found in the comparison between the BR68_FN and BR68 experiments (Figures 2a–2c), but to a far more limited extent.

Ghan et al. (2016) revealed that the LWP is far more susceptible to the increase in aerosols for SPRINTARS with KK00 than for SPRINTARS with BR68. Results here suggest that the larger susceptibility of the LWP to perturbed aerosols for KK00 stems partly from its less efficient depletion of cloud water than BR68 and partly from the feedback from a less efficient wet scavenging of aerosols. This can be traced to the more negative proportional dependency of R_{aut} on N_c for KK00, which ensures its inhibition of rain formation under the condition of a large N_c.

The large wet-scavenging feedback on cloud water and AIE found here underscores the importance to appropriately address the precipitation-aerosol relation in GCMs. Previous studies have found that the precipitation-aerosol relation is likely to be misrepresented by GCMs due to the use of the gridbox-mean, rather than the clear-sky, aerosols in the wet-scavenging process (Weigum et al., 2016; Gryspeerdt et al., 2015), even though there are observational proofs that it is the latter that is more representative of the environment that governs the cloud/precipitation microphysics (Gryspeerdt et al., 2015). GCMs are generally unable to address subgrid aerosol variations, especially that between the clear-sky and the cloud/precipitation portions, giving rise to a potentially overestimated wet-scavenging because of using the less abundant gridbox-mean aerosols in the negative precipitation-N_c relation. This gridbox-mean bias can be more pronounced in regions where precipitation, and hence wet-scavenging, is sufficiently efficient such that the gridbox-mean aerosols can hardly represent the clear-sky environment. And noteworthy, the gridbox-mean bias can be of differing importance to different autoconversion schemes considering their different precipitation-N_c dependencies—schemes with larger precipitation-N_c dependency are supposed to be more susceptible to the gridbox-mean treatment of aerosols. Therefore, to accurately depict the wet-scavenging process and achieve a faithful AIE, the treatments of aerosols, other than the precipitation formation process, should also be improved.

4. Conclusions

Many studies have corroborated a common bias in the warm-precipitation process among state-of-the-art GCMs: specifically, precipitation is triggered too frequently relative to observations. This study, using a particular model (MIROC5.2), found that the onset of warm rain can be improved with respect to satellite observations by altering the formulation of the autoconversion process, which inhibits the triggering of rain under conditions of a large cloud droplet number concentration and small droplet sizes. However, this improvement in warm-rain formation results in an enhanced AIE, to the extent that much of the greenhouse warming in the last century could be offset. Previous studies with other models have also revealed a similar contradiction between "plausible improvement in warm-precipitation formation" and an "implausible energy budget due to enhancement in the AIE." We anticipate this *P&E dichotomy* to be a common feature among those GCMs that trigger warm rain too frequently.

One key cause of the P&E dichotomy in MIROC5.2 is the amplification of the LWP response and resultant AIE through coupling between precipitation formation and the wet scavenging of aerosols. This coupling leads to the following positive feedback mechanism: aerosol-induced inhibition of rain formation causes less efficient wet deposition of aerosols, which induces a larger increase in aerosol loading and cloud droplet number concentration that further inhibits rain and enlarges the cloud water amount. This amplification effect is also expected in other models with the P&E dichotomy, because the restricting of the warm-rain formation process commonly moves clouds with smaller droplet sizes into a regime that features a reduced wet scavenging efficiency and greater susceptibility to aerosol variations. Indeed, the aerosol loadings were also found to significantly differ among varying R_e threshold values in GFDL CM3, arguably due to differing wet-scavenging efficiencies (Suzuki et al., 2017). The different aerosol loadings were also shown to perturb the

atmospheric energy budget, resulting in a significant change in global precipitation. This implies that the P&E dichotomy also matters to the hydrological cycle, as well as the energy budget.

The P&E dichotomy implies that compensating errors exist in the coupling between aerosol, cloud, and precipitation. This underscores the requirement to better constrain other key aerosol-cloud-precipitation processes, particularly wet scavenging, to mediate the overestimated AIE caused by warm-rain formation constraint. Specifically, the biases that could lead to an unrealistic prediction of cloud-water susceptibility to aerosols, which is increasingly indicated by observations to be smaller than or, regionally, even of opposite sign to model predictions (e.g., Malavelle et al., 2017; Sato et al., 2018; Small et al., 2009), should primarily be examined.

Acknowledgments
This study was supported by NOAA's Climate Program Office's Modeling, Analysis, Predictions and Projections program with the grant NA15OAR4310153. K. S. was also supported by JAXA EarthCARE and GCOM-C projects and the Integrated Research Program for Advancing Climate Models (TOUGOU program) from the Ministry of Education, Culture, Sports, Science and Technology (MEXT), Japan. The CloudSat data were obtained from the CloudSat Data Processing Center (DPC) at Colorado State University (http://www.cloudsat.cira.colostate.edu). The MODIS data were obtained from the Level-1 and Atmosphere Archive and Distribution System (LAADS) Distributed Active Archive Center (DAAC) of NASA (https://ladsweb.modaps.eosdis.nasa.gov). The model data are available from http://doi.org/10.5281/zenodo.1184210.

References

Albrecht, B. A. (1989). Aerosols, cloud microphysics, and fractional cloudiness. *Science*, *245*(4923), 1227–1230. https://doi.org/10.1126/science.245.4923.1227

Berry, E. X. (1968). Modification of the warm rain process, paper presented at 1st National Conf. on Weather Modification, April 28–May 1, American Meteorological Society, Albany, New York. pp. 81–85.

Boers, R., Jensen, J. B., & Krummel, P. B. (1998). Microphysical and short-wave radiative structure of stratocumulus clouds over the Southern Ocean: Summer results and seasonal differences. *Quarterly Journal of the Royal Meteorological Society*, *124*(545), 151–168. https://doi.org/10.1002/qj.49712454507

Collins, M., Knutti, R., Arblaster, J., Dufresne, J.-L., Fichefet, T., Friedlingstein, P., et al. (2013). Long-term climate change: Projections, commitments and irreversibility. In *Climate change 2013: The physical science basis. Contribution of Working Group I to the Fifth Assessment Report of the Intergovernmental Panel on Climate Change*, (pp. 1029–1136). Cambridge, United Kingdom and New York, NY, USA: Cambridge University. Press.

Donner, L., O'Brien, T., Rieger, D., Vogel, B., & Cooke, W. (2016). Are atmospheric updrafts a key to unlocking climate forcing and sensitivity? *Atmospheric Chemistry and Physics*, *16*(20), 12,983–12,992. https://doi.org/10.5194/acp-16-12983-2016

Eyring, V., Bony, S., Meehl, G. A., Senior, C. A., Stevens, B., Stouffer, R. J., & et al. (2016). Overview of the Coupled Model Intercomparison Project Phase 6 (CMIP6) experimental design and organization. *Geoscientific Model Development*, *9*(5), 1937–1958. https://doi.org/10.5194/gmd-9-1937-2016

Ghan, S. (2013). Estimating aerosol effects on cloud radiative forcing. *Atmospheric Chemistry and Physics*, *13*(19), 9971–9974. https://doi.org/10.5194/acp-13-9971-2013

Ghan, S., Wang, M., Zhang, S., Ferrachat, S., Gettelman, A., Griesfeller, J., et al. (2016). Challenges in constraining anthropogenic aerosol effects on cloud radiative forcing using present-day spatiotemporal variability. *Proceedings of the National Academy of Sciences of the United States of America*, *113*(21), 5804–5811. https://doi.org/10.1073/pnas.1514036113

Golaz, J.-C., Horowitz, L., & Levy, H. (2013). Cloud tuning in a coupled climate model: Impact on 20th century warming. *Geophysical Research Letters*, *40*, 2246–2251. https://doi.org/10.1002/grl.50232

Golaz, J.-C., Salzmann, M., Donner, L., Horowitz, L., Ming, Y., & Zhao, M. (2011). Sensitivity of the aerosol indirect effect to subgrid variability in the cloud parameterization of the GFDL Atmosphere General Circulation Model AM3. *Journal of Climate*, *24*(13), 3145–3160. https://doi.org/10.1175/2010JCLI3945.1

Gryspeerdt, E., Stier, P., White, B. A., & Kipling, Z. (2015). Wet scavenging limits the detection of aerosol effects on precipitation. *Atmospheric Chemistry and Physics*, *15*(13), 7557–7570. https://doi.org/10.5194/acp-15-7557-2015

Haynes, J. M., L'Ecuyer, T., Stephens, G. L., Miller, S. D., Mitrescu, C., Wood, N. B., & et al. (2009). Rainfall retrievals over the ocean with spaceborne high-frequency cloud radar. *Journal of Geophysical Research*, *114*, D00A22. https://doi.org/10.1029/2008JD009973

Jiang, H., Xue, H., Teller, A., Feingold, G., & Levin, Z. (2006). Aerosol effects on the lifetime of shallow cumulus. *Geophysical Research Letters*, *33*, L14806. https://doi.org/10.1029/2006GL026024

Jing, X., Suzuki, K., Guo, H., Goto, D., Ogura, T., Koshiro, T., & Mülmenstädt, J. (2017). A multimodel study on warm precipitation biases in global models compared to satellite observations. *Journal of Geophysical Research: Atmospheres*, *122*, 11,806–11,824. https://doi.org/10.1002/2017JD027310

Khairoutdinov, M., & Kogan, Y. (2000). A new cloud physics parameterization in a large-Eddy simulation model of marine stratocumulus. *Monthly Weather Review*, *128*(1), 229–243. https://doi.org/10.1175/1520-0493(2000)128<0229:ANCPPI>2.0.CO;2

Malavelle, F. F., Haywood, J., Jones, A., Gettelman, A., Clarisse, L., Bauduin, S., et al. (2017). Strong constraints on aerosol–cloud interactions from volcanic eruptions. *Nature*, *546*(7659), 485–491. https://doi.org/10.1038/nature22974

Marchand, R., Mace, G. G., Ackerman, T., & Stephens, G. (2008). Hydrometeor detection using Cloudsat—An earth-orbiting 94-GHz cloud radar. *Journal of Atmospheric and Oceanic Technology*, *25*(4), 519–533. https://doi.org/10.1175/2007JTECHA1006.1

Matsui, T., Masunaga, H., Kreidenweis, S., Pielke, R., Tao, W., Chin, M., & Kaufman, Y. (2006). Satellite-based assessment of marine low cloud variability associated with aerosol, atmospheric stability, and the diurnal cycle. *Journal of Geophysical Research*, *111*, D17204. https://doi.org/10.1029/2005JD006097

Menon, S., Genio, A., Koch, D., & Tselioudis, G. (2002). GCM simulations of the aerosol indirect effect: Sensitivity to cloud Prameterization and aerosol burden. *Journal of the Atmospheric Sciences*, *59*(3), 692–713. https://doi.org/10.1175/1520-0469(2002)059<0692:GSOTAI>2.0.CO;2

Michibata, T., Suzuki, K., Sato, Y., & Takemura, T. (2016). The source of discrepancies in aerosol–cloud–precipitation interactions between GCM and A-Train retrievals. *Atmospheric Chemistry and Physics*, *16*(23), 15,413–15,424. https://doi.org/10.5194/acp-16-15413-2016

Michibata, T., & Takemura, T. (2015). Evaluation of autoconversion schemes in a single model framework with satellite observations. *Journal of Geophysical Research: Atmospheres*, *120*, 9570–9590. https://doi.org/10.1002/2015JD023818

Myhre, G., Shindell, D., Bréon, F.-M., Collins, W., Fuglestvedt, J., Huang, J., et al. (2013). Anthropogenic and natural radiative forcing. In *Climate change 2013: The physical science basis. Contribution of Working Group I to the Fifth Assessment Report of the Intergovernmental Panel on Climate Change*, (pp. 659–740). Cambridge, United Kingdom and New York, NY, USA: Cambridge Univ. Press.

Nakajima, T. Y., Suzuki, K., & Stephens, G. L. (2010). Droplet growth in warm water clouds observed by the A-Train. Part II: A multisensor view. *Journal of the Atmospheric Sciences*, *67*(6), 1897–1907. https://doi.org/10.1175/2010JAS3276.1

Pawlowska, H., & Brenguier, J.-L. (2003). An observational study of drizzle formation in stratocumulus clouds for general circulation model (GCM) parameterizations. *Journal of Geophysical Research*, *108*(D15), 8630. https://doi.org/10.1029/2002JD002679

Platnick, S., Ackerman, S. A., King, M. D., Meyer, K., Menzel, W. P., Holz, R. E., et al. (2015). MODIS atmosphere L2 cloud product (06_L2), NASA MODIS Adaptive Processing System, Goddard Space Flight Center. https://doi.org/10.5067/MODIS/MOD06_L2.006

Rotstayn, L. D. (2000). On the "tuning" of autoconversion parameterizations in climate models. *Journal of Geophysical Research*, *105*(D12), 15,495–15,507. https://doi.org/10.1029/2000JD900129

Rotstayn, L. D., Collier, M. A., Shindell, D. T., & Boucher, O. (2015). Why does aerosol forcing control historical global-mean surface temperature change in CMIP5 models? *Journal of Climate*, *28*(17), 6608–6625. https://doi.org/10.1175/JCLI-D-14-00712.1

Sato, Y., Goto, D., Michibata, T., Suzuki, K., Takemura, T., Tomita, H., & Nakajima, T. (2018). Aerosol effects on cloud water amounts were successfully simulated by a global cloud-system resolving model. *Nature Communications*, *9*(1), 985. https://doi.org/10.1038/s41467-018-03379-6

Small, J. D., Chuang, P. Y., Feingold, G., & Jiang, H. (2009). Can aerosol decrease cloud lifetime? *Geophysical Research Letters*, *36*, L16806. https://doi.org/10.1029/2009GL038888

Stephens, G. L., L'Ecuyer, T., Forbes, R., Gettlemen, A., Golaz, J. C., Bodas-Salcedo, A., et al. (2010). Dreary state of precipitation in global models. *Journal of Geophysical Research*, *115*, D24211. https://doi.org/10.1029/2010JD014532

Stevens, B., & Feingold, G. (2009). Untangling aerosol effects on clouds and precipitation in a buffered system. *Nature*, *461*, 7264.

Storelvmo, T., Kristjánsson, J., Lohmann, U., Iversen, T., Kirkevåg, A., & Seland, Ø. (2008). Modeling of the Wegener–Bergeron–Findeisen process—Implications for aerosol indirect effects. *Environmental Research Letters*, *3*(4), 045001.

Suzuki, K., Golaz, J., & Stephens, G. (2013). Evaluating cloud tuning in a climate model with satellite observations. *Geophysical Research Letters*, *40*, 4464–4468. https://doi.org/10.1002/grl.50874

Suzuki, K., Nakajima, T. Y., & Stephens, G. L. (2010). Particle growth and drop collection efficiency of warm clouds as inferred from joint CloudSat and MODIS observations. *Journal of the Atmospheric Sciences*, *67*(9), 3019–3032. https://doi.org/10.1175/2010JAS3463.1

Suzuki, K., Stephens, G. L., Bodas-Salcedo, A., Wang, M., Golaz, J.-C., Yokohata, T., & Tsuyoshi, K. (2015). Evaluation of the warm rain formation process in global models with satellite observations. *Journal of the Atmospheric Sciences*, *72*(10), 3996–4014. https://doi.org/10.1175/JAS-D-14-0265.1

Suzuki, K., Stephens, G. L., & Golaz, J.-C. (2017). Significance of aerosol radiative effect in energy balance control on global precipitation change. *Atmospheric Science Letters*, *18*(10), 389–395. https://doi.org/10.1002/asl.780

Swales, D. J., Pincus, R., & Bodas-Salcedo, A. (2018). The cloud feedback model intercomparison project observational simulator package: Version 2. *Geoscientific Model Development*, *11*(1), 77–81. https://doi.org/10.5194/gmd-11-77-2018

Takahashi, H., Lebsock, M., Suzuki, K., Stephens, G., & Wang, M. (2017). An investigation of microphysics and subgrid-scale variability in warm-rain clouds using the A-Train observations and a multiscale modeling framework. *Journal of Geophysical Research: Atmospheres*, *122*, 7493–7504. https://doi.org/10.1002/2016JD026404

Takemura, T., Egashira, M., Matsuzawa, K., Ichijo, H., O'ishi, R., & Abe-Ouchi, A. (2009). A simulation of the global distribution and radiative forcing of soil dust aerosols at the Last Glacial Maximum. *Atmospheric Chemistry and Physics*, *9*(9), 3061–3073. https://doi.org/10.5194/acp-9-3061-2009

Wang, M., Ghan, S., Ovchinnikov, M., Liu, X., Easter, R., Kassianov, E., et al. (2011). Aerosol indirect effects in a multi-scale aerosol-climate model PNNL-MMF. *Atmospheric Chemistry and Physics*, *11*(11), 5431–5455. https://doi.org/10.5194/acp-11-5431-2011

Watanabe, M., Suzuki, T., O'ishi, R., Komuro, Y., Watanabe, S., Emori, S., et al. (2010). Improved climate simulation by MIROC5: Mean states, variability, and climate sensitivity. *Journal of Climate*, *23*(23), 6312–6335. https://doi.org/10.1175/2010JCLI3679.1

Weigum, N., Schutgens, N., & Stier, P. (2016). Effect of aerosol subgrid variability on aerosol optical depth and cloud condensation nuclei: Implications for global aerosol modelling. *Atmospheric Chemistry and Physics*, *16*(21), 13,619–13,639. https://doi.org/10.5194/acp-16-13619-2016

Zhao, M., Golaz, J.-C., Held, I., Guo, H., Balaji, V., Benson, R., et al. (2018). The GFDL global atmosphere and land model AM4.0/LM4.0: 2. Model description, sensitivity studies, and tuning strategies. *Journal of Advances in Modeling Earth Systems*, *10*, 735–769. https://doi.org/10.1002/2017MS001209